Appl Phys A (2009) 96: 691–699
DOI 10.1007/s00339-009-5151-0

Applied Physics A
Materials Science & Processing

A simple thermal decomposition synthesis, magnetic properties, and cytotoxicity of $La_{0.7}Sr_{0.3}MnO_3$ nanoparticles

Sujittra Daengsakul · Charusporn Mongkolkachit · Chunpen Thomas · Sineenat Siri · Ian Thomas · Vittaya Amornkitbamrung · Santi Maensiri

Received: 2 December 2008 / Accepted: 9 February 2009 / Published online: 6 March 2009

Abstract This study reports the new and simple synthesis of magnetic $La_{0.7}Sr_{0.3}MnO_3$ (LSMO) nanoparticles by thermal decomposition method using acetate salts of La, Sr and Mn as starting materials. To obtain the LSMO nanoparticles, thermal decomposition of the precursor is carried out at the temperatures of 600, 700, 800, 900, and 1000°C for 6 hours. The synthesized LSMO nanoparticles were characterized by XRD, FT-IR, TEM and SEM. Structural characterization shows that the prepared particles consisted of two phases of $LaMnO_3$ (LMO) and LSMO with crystallite sizes ranging from 18 to 55 nm. All the prepared samples have a perovskite structure which changes from cubic to rhombohedral with the increase in the thermal decomposition temperature. Basic magnetic characteristics such as saturation magnetization (M_S) and coercive field (H_C) are evaluated by sample vibrating magnetometry at room temperature (20°C). The samples show soft ferromagnetic behavior with M_S values of ∼9–55 emu/g and H_C values of ∼8–37 Oe, depending on the crystallite size and thermal decomposition temperature. The relationship between the crystallite size and the magnetic properties is presented and discussed. The cytotoxicity of synthesized LSMO nanoparticles was also evaluated with NIH 3T3 cells and the result showed that the synthesized nanoparticles were not toxic to the cells as determined from cell viability in response to the liquid extraction of LSMO nanoparticles.

PACS 61.05.Cp · 75.47.Lx · 75.50.Tt · 81.07.Bc · 81.10.Dn · 81.16.Be · 81.20.Ka · 81.70.Pg

S. Daengsakul · C. Thomas · I. Thomas · V. Amornkitbamrung · S. Maensiri (✉)
Department of Physics, Faculty of Science, Khon Kaen University, Khon Kaen 40002, Thailand
e-mail: sanmae@kku.ac.th

S. Maensiri
e-mail: santimaensiri@gmail.com

S. Daengsakul · C. Thomas · S. Siri · I. Thomas · V. Amornkitbamrung · S. Maensiri
Integrated Nanotechnology Research Center (INRC), Khon Kaen University, Khon Kaen 40002, Thailand

C. Mongkolkachit
National Metal and Materials Technology Center (MTEC) 114 Thailand Science Park, Paholyothin, Klong Luang, Pathumthan 12120, Thailand

S. Siri
Department of Biochemistry, Faculty of Science, Khon Kaen University, Khon Kaen 40002, Thailand

1 Introduction

The perovskite manganites $A_{1-x}B_xMnO_3$, where A is a trivalent lanthanide cation (e.g., La) and B is a divalent cation (e.g., Ca, Sr, Ba, and Pb), have recently attracted much attention because of their technical applications [1–3]. Among others, Sr-doped $LaMnO_3$ or LSMO is particularly of interest due to its good magnetic, electrical and catalytic properties. LSMO with nominal composition $La_{0.7}Sr_{0.3}MnO_3$ showed a better performance as compared to other compositions and therefore it becomes the research emphasis in this material system. A variety of methods have been developed to prepare $La_{0.7}Sr_{0.3}MnO_3$ nanoparticles, including sol–gel route [4], molten salt method [5], autocombustion process [6], hydrothermal synthesis [7], to name just a few. Among these established synthesis methods, it is still critical to find simple and cost effective routes

to synthesize nanocrystalline $La_{0.7}Sr_{0.3}MnO_3$ by utilization of cheap, nontoxic and environmentally benign precursors. Recently, our group has reported the synthesis of ZnO nanoparticles with crystallite sizes of 30–40 nm by a direct thermal decomposition of zinc acetate in air at 400–700°C for 4 h [8]. The method is fast, simple, and cost effective, which is a promising synthesis route for preparations of metal oxide and complex oxide nanoparticles.

In this paper, we demonstrate the applicability of a direct thermal decomposition to the preparation of $La_{0.7}Sr_{0.3}MnO_3$ nanoparticles. The prepared samples were characterized by thermogravimetric-differential analysis (TG-DTA), X-ray diffraction (XRD), Fourier transmission infrared (FT-IR) spectroscopy, scanning electron microscopy (SEM) and transmission electron microscopy (TEM). The magnetic properties of the samples were investigated by a vibrating sample magnetometer (VSM). The effects of crystallite size on the magnetic properties were also discussed in detail.

2 Experimental Details

High purity acetates of $La(CH_3COO)_3.xH_2O$ (99.9%, Aldrich), $Sr(CH_3COO)_2$ (99%, Aldrich) and $Mn(CH_3COO)_2.4H_2O$ (>99.9%, Fluka) were used as starting materials. In a typical procedure, 0.007 mol metal acetates with a mole ratio corresponding to the nominal composition of La:Sr:Mn ratio of 0.7:0.3:1 were dissolved in deionized water (DI water) at a ratio of 5:1 (volume(ml)/weight(g)) of DI water to total acetate salts. The mixed solution was stirred with a magnetic stirrer at room temperature for 15 min, and was thermally decomposed in an oven under normal atmosphere at different temperatures from 600–1000°C for 6 h and left to cool down to room temperature before being ground to obtain LSMO nanoparticles.

To better understand the thermal stability, decomposition temperature and mechanism of the thermal decomposition, two precursors of the mixed metal acetates in DI water (precursor A) and the mixed ground metal acetates without water (precursor B) were characterized by TG/DTA at 10°C min^{-1} from 25 to 1000°C (NETZSCH, STA449C Jupiter).

There is no characterization of the crystal structure in this paper. Only powder diffractograms are shown for the purpose of analysis of crystalline phase. The crystal structure of the synthesized $La_{0.7}Sr_{0.3}MnO_3$ nanoparticles was characterized by X-ray diffraction (XRD) (Philips PW3040, The Netherlands) with the crystallite size calculated from the broadening of the XRD peaks using the Scherrer's equation. The functional groups present in the samples were studied using the Fourier transform infrared Spectroscopy technique (FT-IR) (Spectrum one, Perkin Elmer Instrument, USA). The samples were incorporated in KBr pellets of which the FT-IR spectra were obtained in the 1200–450 cm^{-1} wavenumber range. The morphology of the samples was revealed by scanning electron microscopy (SEM) (LEO 1450VP, UK) and transmission electron microscopy (TEM) (JEOL 2010, 200 kV, Japan). The selected area electron diffraction (SAED) patterns from TEM were analyzed to identify the phase and to confirm the results obtained from XRD. The magnetic properties were investigated by a Vibrating Sample Magnetometer (VSM) (Lakeshore 7403, USA) at room temperature (20°C).

The cytotoxicity of $La_{0.7}Sr_{0.3}MnO_3$ nanoparticles was evaluated with NIH 3T3 and cell viability was determined by MTT colorimetric assay (Sigma, USA). Cells were seeded on the 96-well culture plate (1×10^4 cells/well) for 24 h. The extracted $La_{0.7}Sr_{0.3}MnO_3$ liquid was performed in sterile distilled water at 121°C for 1 h with the ratio of 0.2 g/ml. Cells were incubated with 20 µl extracted $La_{0.7}Sr_{0.3}MnO_3$ liquid or sterile water (control) for 24 h. After removed the medium, 10 µl of 12 mM MTT solution was added and incubated for further 4 h. Blue formazan crystals, metabolized MTT in mitochondria of viable cells, were dissolved in 50 µl of dimethylsulfoxide (DMSO; Sigma, USA) and measured at 550 nm by the plate reader (Biorad, Japan). The average value of 4 wells was used for each sample and two repeats were done in each experiment. The control NIH 3T3 cell viability was defined as 100%. Statistical comparison was performed using one-way ANOVA with SPSS software version 11.5 (SPSS, Germany).

3 Results and discussions

3.1 Thermal analysis

The TG/DTA results of the precursor A and precursor B in Fig. 1 show that precursor A (Fig. 1(a)) lost its weight in three different steps. The most prominent step took place from 50 to 200°C with ca. 87% weight loss, which was presumably due to thermal dehydration of La, Sr and Mn acetate hydrates. The second step (from 200 to 400°C) was related to the release of organic compounds such as acetone [CH_3COCH_3]. In this range of temperature, the acetates are decomposed into carbonates and oxycarbonate. These decompositions took place in the temperatures between 250 and 400°C, and the possible decomposition processes are as follows [9, 10]:

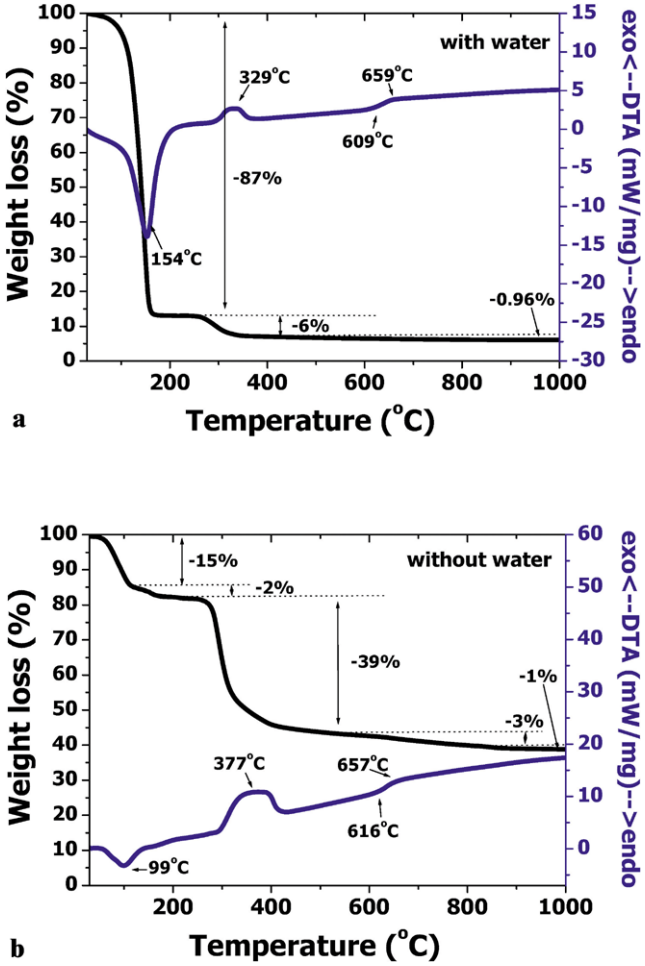

Fig. 1 TG/DTA curves of (**a**) the solution of metal acetates in DI water (precursor A) and (**b**) the mixed ground metal acetates without water (precursor B)

$$\left.\begin{aligned}
&0.7La(CH_3COO)_3.1.5H_2O \\
&\quad \rightarrow 0.7LaCO_3(CH_3CO_2) + 1.05H_2O\uparrow \\
&\qquad + 0.7CH_3COCH_3\uparrow \\
&0.7LaCO_3(CH_3CO_2) \\
&\quad \rightarrow 0.35La_2O_2CO_3 + 0.35CH_3COCH_3\uparrow \\
&\qquad + 0.7CO_2\uparrow \\
&0.3Sr(CH_3COO)_2 \rightarrow 0.3SrCO_3 + 0.3CH_3COCH_3\uparrow \\
&Mn(CH_3COO)_2.4H_2O \\
&\quad \rightarrow Mn(CH_3COO)_2 + 4H_2O\uparrow \\
&\quad \rightarrow MnCO_3 + CH_3COCH_3\uparrow
\end{aligned}\right\} \quad (1)$$

The third step, from 500 to 900°C, was due to the loss of CO_2 molecules. In this step, the carbonates ($SrCO_3$, $MnCO_3$) and oxycarbonate ($La_2O_2CO_3$) were decomposed into La_2O_3, SrO, and MnO with emission of CO_2 corresponding to the mechanism of decomposition as follows [11]:

$$\left.\begin{aligned}
&0.35La_2O_2CO_3 \rightarrow 0.35La_2O_3 + CO_2\uparrow \\
&\quad \rightarrow 0.35La_2O_3 \\
&0.3SrCO_3 \rightarrow 0.3SrO + 0.3CO_2\uparrow \\
&MnCO_3 \rightarrow MnO + CO_2\uparrow \\
&\quad \rightarrow \textit{reduction} \rightarrow 0.3MnO_2 + 0.35Mn_2O_3
\end{aligned}\right\} \quad (2)$$

The formation of $MnCO_3$ from $Mn(CH_3COO)_2.4H_2O$ is probably due to a reduction of Mn ($Mn^{3+} \rightarrow Mn^{2+}$) [12]. Consequently, the thermal decomposition of most of Mn acetate in air (in the temperature range 250–330°C) leads normally to the formation of mixed oxides of MnO_2, Mn_2O_3 and Mn_3O_4. It is known that the differences in oxalate hydrate stoichiometries and environments can result in the formation of different Mn oxide products [13]. Therefore, the possible formation of the prepared LSMO in our study is as follows:

$$\left.\begin{aligned}
&La_2O_3 + Mn_2O_3 \rightarrow 2LaMnO_3 \\
&SrO + MnO_2 \rightarrow SrMnO_3 \\
&0.35(La_2O_3 + Mn_2O_3) + 0.3(SrO + MnO_2) \\
&\quad \rightarrow La_{0.7}Sr_{0.3}MnO_3
\end{aligned}\right\} \quad (3)$$

The possible thermal decompositions of La, Sr and Mn acetate salts and formation of the LSMO are given by the reactions (1), (2), and (3), respectively. Similar behavior was observed for precursor B (Fig. 1(b)), but in the last step, the decomposition of precursor B still continued. It is noted that dissolving the metal acetates in DI water results in a better mixture of La, Sr and Mn acetate salts, making the mixture of the precursor A more homogeneous than that of the precursor B.

3.2 Structural characterization

The XRD results of the $La_{0.7}Sr_{0.3}MnO_3$ nanoparticles prepared by thermal decomposition of the precursor A and B at 800°C for 6 h are shown in Fig. 2. Both samples show a main phase of LSMO, but the sample prepared using precursor B contains a large amount of impurities $La(OH)_3$ and $SrCO_3$ (Fig. 2(b)). In this study, we therefore focus on the LSMO nanoparticles prepared using the precursor A. Figure 3 shows the XRD results of the samples prepared by thermal decomposition of the precursor A in air at 600, 700, 800, 900, and 1000°C for 6 hours. The presence of impurities phases such as $SrCO_3$ (JCPD no. 05-0418), $La_2O_2CO_3$ (JCPD no. 37-0804) and $La(OH)_3$ (JCPD no. 36-1481) was observed in the samples thermally decomposed below 800°C, while above 800°C the samples exhibited a pure phase of LSMO. The transformation of the crystal structure from cubic to rhombohedral occurred at and above 900°C.

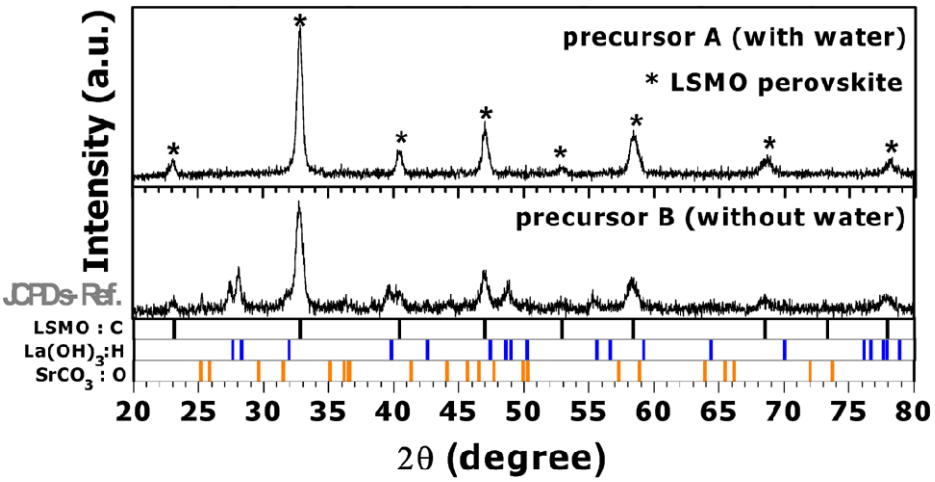

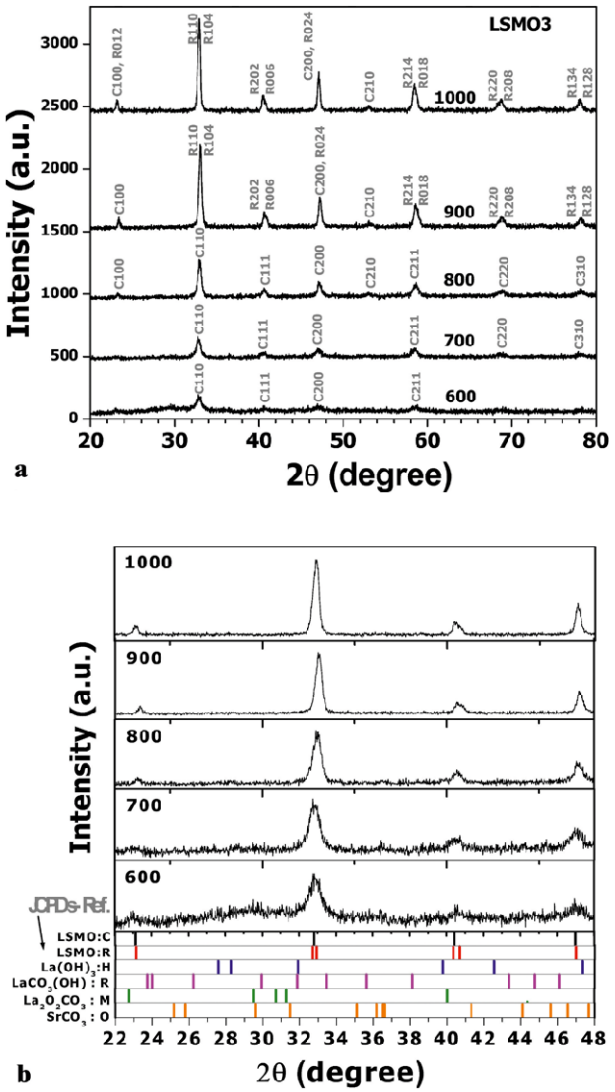

Fig. 2 XRD patterns of the $La_{0.7}Sr_{0.3}MnO_3$ nanoparticles prepared by thermal decomposition of (**a**) precursor A and (**b**) precursor B at 800°C for 6 h

Fig. 3 XRD patterns of the $La_{0.7}Sr_{0.3}MnO_3$ nanoparticles prepared by thermal decomposition of the precursor A at 600, 700, 800, 900, and 1000°C for 6 h. (**a**) $2\theta = 20$–80 degrees (**b**) $2\theta = 22$–48 degrees (R and C identify as rhombohedral and cubic phase, respectively) or (R: rhombohedral phase and C: cubic phase)

The particle sizes of the synthesized samples estimated using Scherrer's equation (Table 1) were 18, 24, 40 and 55 nm for the samples thermally decomposed at 700, 800, 900, and 1000°C, respectively. It is clearly seen that the particle size increases with increasing thermal decomposition temperature.

Figure 4 shows the FT-IR spectra of the standard KBr and the samples prepared at 600–1000°C for 6 hours. The band around 600 cm^{-1} corresponds to the stretching mode, which involves the internal motion of a change in Mn–O–Mn bond length [14]. This band is related to the environment surrounding the MnO_6 octahedral. For the samples prepared below 800°C, the small absorption bands at around 860–900 cm^{-1} were observed. These bands correspond to $SrCO_3$, $La_2O_2CO_3$ and $LaCO_3(OH)$ impurity peaks which disappeared at higher temperature of thermal decomposition. The FT-IR results agree well with the XRD results (Fig. 3).

3.3 Morphologies

The detailed morphologies of the prepared samples revealed by SEM and TEM are presented in Figs. 5 and 6, respectively. The SEM micrographs (Fig. 5) show that the prepared samples consisted of agglomerated nanoparticles with particle sizes of ca. 50–300 nm. The particle size increases with an increase in thermal decomposition temperature. From the TEM images (Fig. 6), the particle sizes of the prepared samples are in the range of 20–60 nm, which increase as the thermal decomposition temperature increases, in good agreement with those estimated from XRD line-broadening. The corresponding SAED patterns in Fig. 6 show spotty ring patterns, suggesting their polycrystalline structure in all the prepared LSMO samples. An increase in thermal decomposition temperature results in stronger spotty pattern, indicating larger particle size with highly crystalline structure. This is in agreement with the XRD results (Fig. 3). These results also confirm the transformation of crystal structure from cubic to rhombohedral as the thermal decomposition temper-

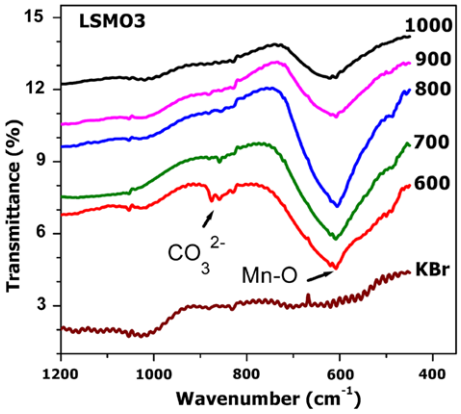

Fig. 4 FT-IR spectra of the $La_{0.7}Sr_{0.3}MnO_3$ nanoparticles prepared by thermal decomposition of the precursor A at 600, 700, 800, 900, and 1000°C for 6 h

ature increases to and above 900°C. Note that traces of impurity phase of $La(OH)_3$ are found with TEM technique in the sample prepared at 1000°C, while they are not detected in XRD pattern in Fig. 3.

3.4 Magnetic properties

The specific magnetization curves obtained from VSM measurements shown in Fig. 7 indicate a ferromagnetic behavior in all the samples. The specific magnetization (M_S) decreases with a decrease in thermal decomposition temperature, i.e., a decrease in particle size. The change in M_S may be due to a structural transformation when the rhombohedral phase transforms into the orthorhombic phase, the Mn–O–Mn bond angle becomes smaller [15] and the smaller Mn–O–Mn bond angles tend to reduce magnetization [16]. Thus, in this study, the decrease in M_S may be due to the decrease in Mn–O–Mn bond angle in the MnO_6 octahe-

Table 1 Properties of the prepared $La_{0.7}Sr_{0.3}MnO_3$ nanoparticles

$La_{0.7}Sr_{0.3}MnO_3$				
Thermal decomposition temperature (°C)	700	800	900	1000
Crystal structure	Cubic	Cubic	Cubic + Rhombohedral	Cubic + Rhombohedral
Particles size (nm)	18	24	40	55
Saturation Magnetization M_S (emu/g)	9.93	25.17	46.76	54.96
Coercivity H_C (Oe)	8.65	22.2	39.4	37.1

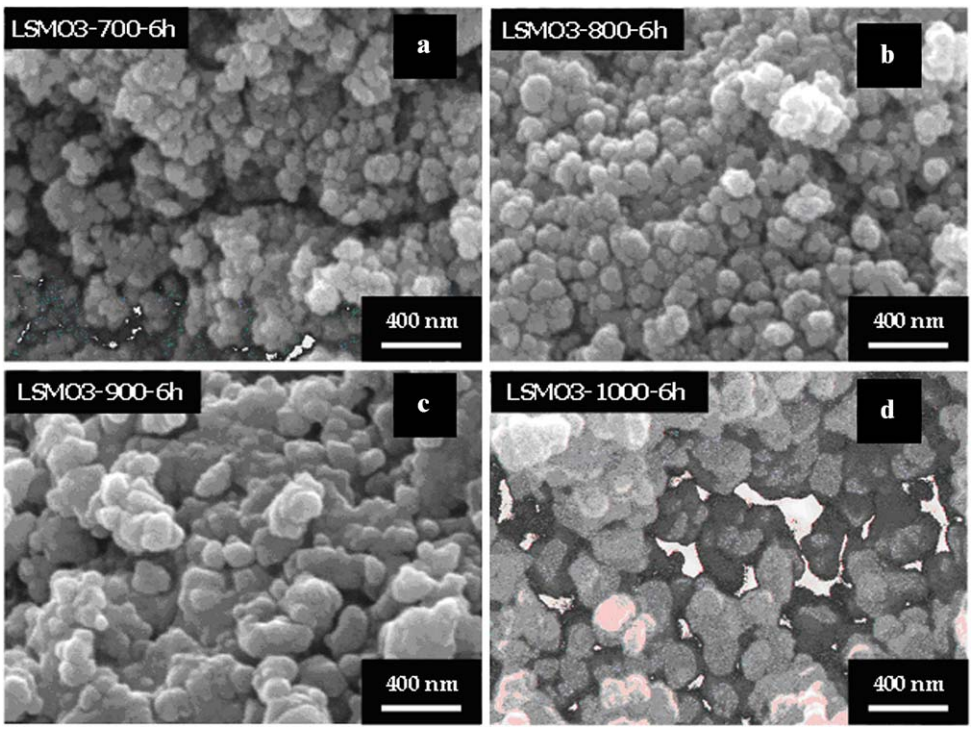

Fig. 5 SEM micrographs of the $La_{0.7}Sr_{0.3}MnO_3$ nanoparticles prepared by thermal decomposition of the precursor A at (**a**) 700°C, (**b**) 800°C, (**c**) 900°C, and (**d**) 1000°C for 6 h

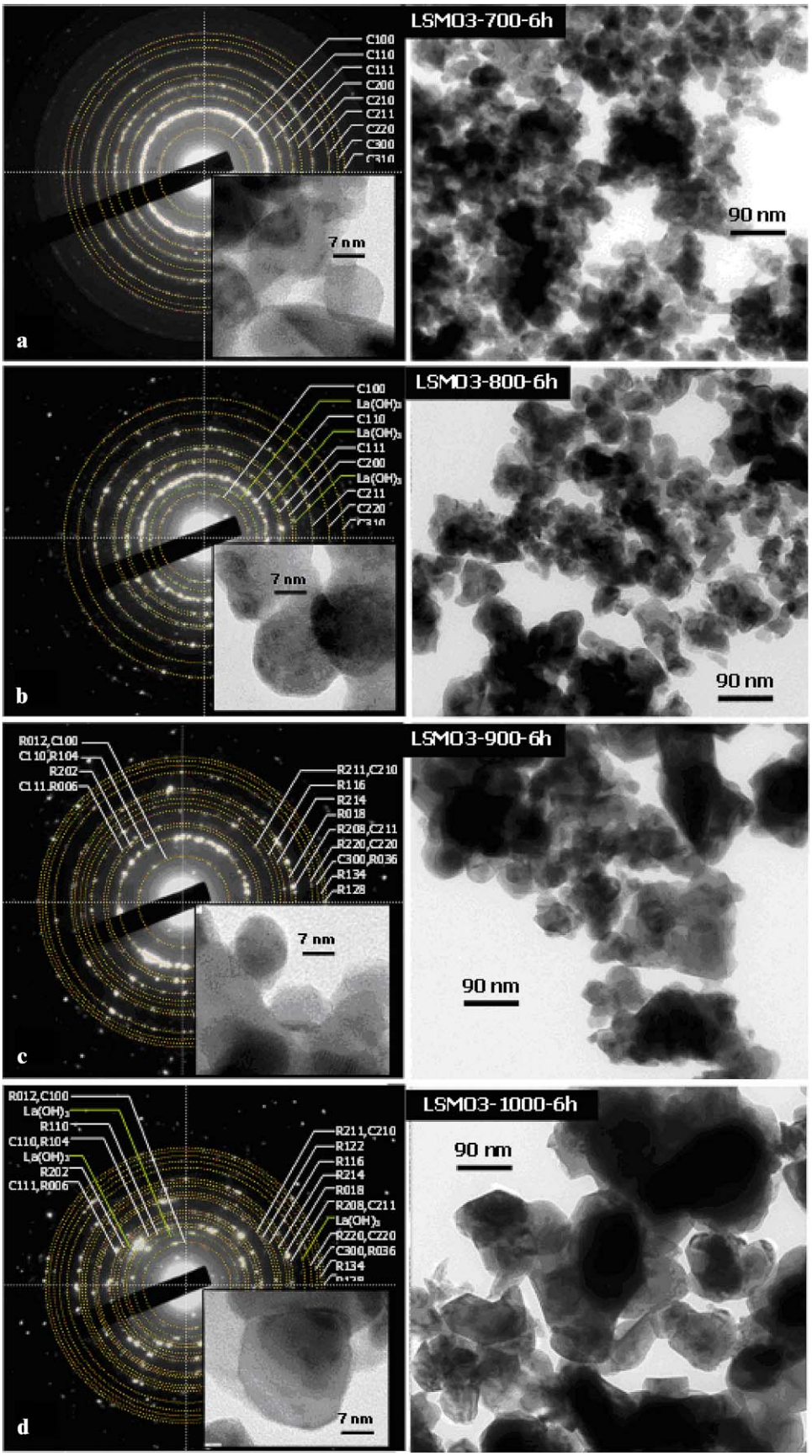

Fig. 6 TEM images with corresponding SAED patterns of the $La_{0.7}Sr_{0.3}MnO_3$ nanoparticles thermally decomposed at (**a**) 700°C, (**b**) 800°C, (**c**) 900°C, and (**d**) 1000°C for 6 h

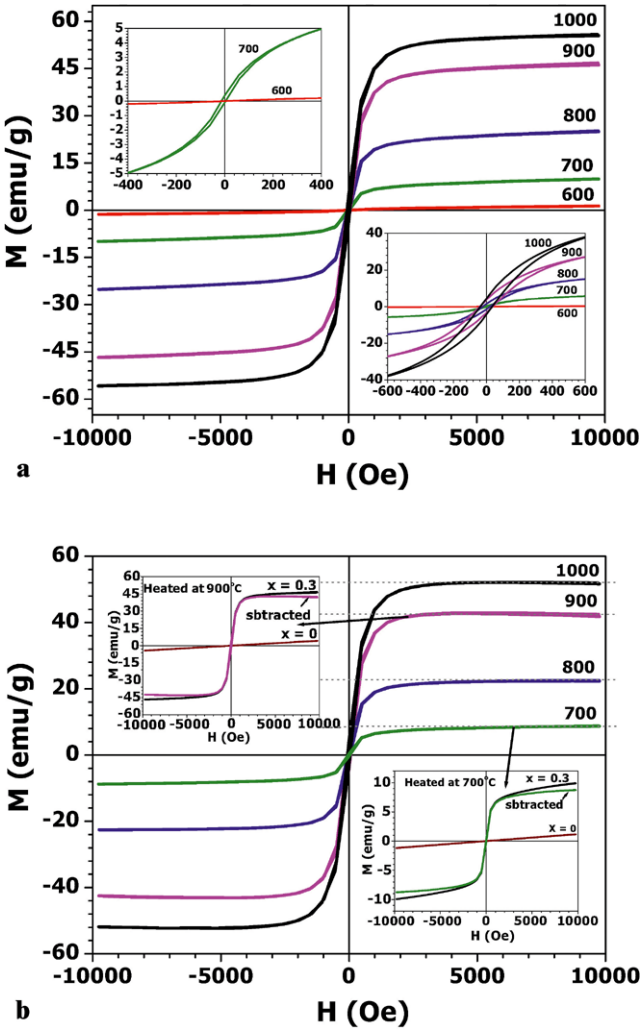

Fig. 7 Room temperature M vs. H of the $La_{0.7}Sr_{0.3}MnO_3$ nanoparticles prepared by thermal decomposition of the precursor A at 600, 700, 800, 900, and 1000°C for 6 h before and after subtraction by $LaMnO_3$ prepared with the same method and condition: (**a**) before subtraction, (**b**) after subtraction (*inset (a)* shows their hysteresis loop and *inset (b)* shows the subtraction of the M–H curve of the $La_{0.7}Sr_{0.3}MnO_3$ nanoparticles prepared at 700 and 900°C by $LaMnO_3$, respectively)

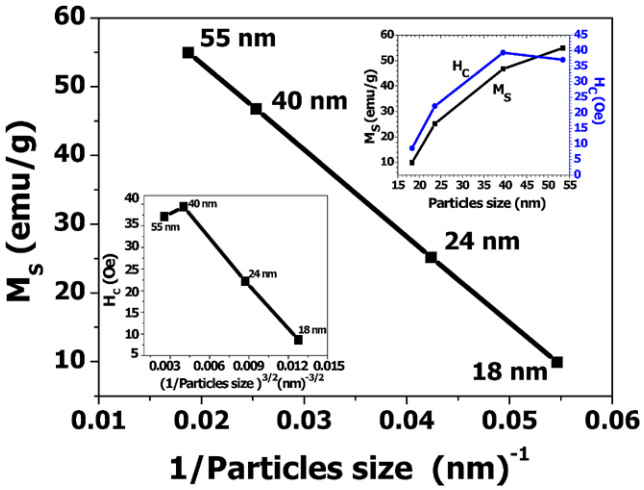

Fig. 8 The plot of M_S versus 1/(particle size) for the $La_{0.7}Sr_{0.3}MnO_3$ nanoparticles. The *inset on the left* is a plot of the H_C versus 1/(particle size)$^{3/2}$, and the *inset on the right* is a plot of the M_S versus particle size

dron as the structure changes from rhombohedral to cubic.

The observation of the M–H curves in Fig. 7(a) shows no saturation of M_S in the range of applied field measurement (±10 kOe). There are two possible reasons that would explain this phenomenon: (i) the applied magnetic field H is not high enough to make the magnetization of LSMO samples saturated; (ii) there is the paramagnetic phase contamination in the samples. It is well known that the Sr doping into $LaMnO_3$ perovskite structure turns the sample ferromagnetic at room temperature. Therefore, we subtracted the M–H curve of the LSMO from the one of the $LaMnO_3$ which was prepared using the same method and condition. The results (inset in Fig. 7(b)) show that there is only the paramagnetic phase of $LaMnO_3$ presented in the samples prepared above 900°C. In the case of the samples prepared below 900°C, there is still no saturation even after subtraction of the M–H curve of $LaMnO_3$. This may be due to the presence of the other paramagnetic phases such as $La(OH)_3$ (detected by TEM) in the samples. These results indicate the presence of incomplete substitutions of Sr for La site in perovskite structure.

Figure 8 shows the plot of saturated magnetization M_S versus the inverse of particle size of the $La_{0.7}Sr_{0.3}MnO_3$ nanoparticles. It is clearly seen in the inset of Fig. 8 (right) that the M_S decreases with the increase in the particle size. In a granular perovskite system, a grain of the perovskite can be assumed to be a two-phase system, a body and a surface. The body phase would have the same properties as the bulk compound such as magnetic and transport properties, but the surface phase would have low transition temperature and magnetization [17]. A decrease in M_S with decreasing crystallize size in Fig. 8 may be attributed to the existence of a nonmagnetic surface layer or to a non-collinear spin arrangement at the surface of the crystal which is a consequence of a so-called magnetically dead layer. The increase of magnetically disordered states at the surface of a crystal can be due to the termination of the crystal structure, breaking of Mn–O–Mn paths, deviation of stoichiometric composition, oxygen vacancies and dislocation [17]. Therefore, the linear dependence of M_S with the inverse of the mean crystallite size observed in our $La_{0.7}Sr_{0.3}MnO_3$ nanoparticles is a clear indication that the reduction in the M_S is only a function of the crystallite size, and this suggests that the magnetically dead layer is approximately the same for all the samples [18].

It is known that ferromagnetic particles with diameter smaller than a critical size have single-magnetic domain

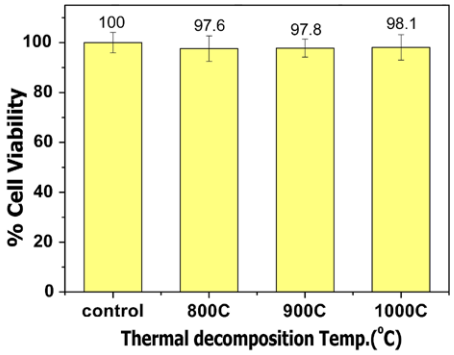

Fig. 9 Cytotoxcity of $La_{0.7}Sr_{0.3}MnO_3$ nanoparticles at the calcination conditions of 800, 900, and 1000°C was studied on NIH 3T3 cells. Cells were incubated with the liquid extractions of nanoparticles or water (control) for 24 h before cell viability was determined by MTT assay

behavior with H_C exhibiting a (crystallite size)$^{-3/2}$ dependence [19]. It can be seen from the inset of Fig. 8 (left) that the H_C varies linearly with the inverse of the (mean crystallite size)$^{3/2}$ when the particle size is below 40 nm. This indicates that the samples with the crystallite size smaller than 40 nm should be single magnetic domain, whereas the sample with particle size greater than 40 nm has multi-ferromagnetic domains. Therefore, the critical particle size of our LSMO samples is around 40 nm. This is quite smaller than the critical diameter value of 80 nm for manganite reported by Sanchez et al. [20]. The properties of the prepared samples in this study are summarized in Table 1.

3.5 Cytotoxicity of the nanoparticles

To evaluate the cytotoxicity of the $La_{0.7}Sr_{0.3}MnO_3$ nanoparticles prepared at the calcination conditions of 800, 900 and 1000°C, the extracted liquid of $La_{0.7}Sr_{0.3}MnO_3$ nanoparticles was incubated with NIH 3T3 for 24 h and cell viability in response to the extracted liquid was evaluated by MTT assay. Negative control was also included by incubating cells with water and the cell viability of the negative control was determined as 100%. The result showed that $La_{0.7}Sr_{0.3}MnO_3$ nanoparticles were not toxic to the cells. Cell viability in response to liquid extraction of $La_{0.7}Sr_{0.3}MnO_3$ nanoparticles was 97.6, 97.7 and 98.1%, respectively, which was not significantly different from the cell viability of the negative control (Fig. 9).

4 Conclusions

$La_{0.7}Sr_{0.3}MnO_3$ nanoparticles with particle sizes of 18–55 nm have been synthesized by a simple thermal decomposition method using acetate salts in DI water. The structural characterization showed that the prepared particles consist of two main phases of $LaMnO_3$ and $La_{0.7}Sr_{0.3}MnO_3$. All the prepared samples have a perovskite structure which changes from cubic to rhombohedral with the increase in the thermal decomposition temperature. The study of magnetic properties at room temperature show that M_S and H_C depend strongly on the particle size. The magnetic measurement results indicate that there is an incomplete substitution of Sr for La site in perovskite structure. The samples show a soft ferromagnetic behavior with M_S values of ~9–55 emu/g and H_C values of ~8–37 Oe, depending on the crystallite size and thermal decomposition temperature. The samples with the crystallite size smaller than 40 nm contain single magnetic domain particles, whereas the sample with particle size larger than 40 nm has multi-ferromagnetic domains. In addition, the magnetic nanoparticles showed no toxicity to the tested cells, NIH 3T3, as determined from the result of cell viability in response to the liquid extraction of the magnetic nanoparticles. This may be useful for medical applications. The present work proves that the hydrothermal decomposition is a new useful method for preparation of manganite nanoparticles, and gives a potential avenue for further practical scale-up of the production process and applications.

Acknowledgements The authors would like to thank the Department of Chemistry of Khon Kaen University for providing FT-IR and VSM facilities, the Faculty of Science Electron Microscopy Unit for providing SEM facilities, and the National Metal and Materials Technology Center (MTEC) of NSTDA for providing TG/DTA and TEM facilities. S. Daengsakul would like to thank the TGIST scholarship for the support of her Ph.D. study. This work is financially supported by The National Research Council of Thailand (NRCT) under the research contract no. PorKor/2550-287.

References

1. J. Heremans, J. Phys. D **26**, 1149 (1993)
2. C.N.R. Rao, B. Raveau, in *Colossal Magnetoresistance, Charge Ordering and Related Properties and Manganese Oxides*, ed. by C.N.R. Rao, B. Raveau (World Scientific, Singapore, 1998)
3. K. Dorr, J. Phys. D Appl. Phys. **39**, R125 (2006)
4. M. Gaudon, C. Laberty-Robert, F. Ansart, P. Stevens, A. Rousset, Solid State Sci. **4**, 125 (2002)
5. Y. Tain, D. Chen, X. Jiao, Chem. Mater. **18**, 6088 (2006)
6. B.M. Nagabhushana, R.P.S. Chakradhar, K.P. Ramesh, C. Shivakumara, G.T. Chandrapp, Mater. Res. Bull. **41**, 1735 (2006)
7. C. Li, T. Li, B. Wang, H. Yan, J. Cryst. Growth **295**, 137 (2006)
8. S. Labauyai, P. Proarak, S. Maensiri, Appl. Phys. A: Mater. Sci. Process. (in press)
9. K.C. Patil, G.V. Chandrashekhar, M.V. George, C.N.R. Rao, Can. J. Chem. **46**, 257 (1968)
10. L. Fabbrini, I. Rossetti, L. Forni, Appl. Catal. B **56**, 223 (2005)
11. C. Vazquez-Vazquez, M.A. Lopez-Quintela, J. Solid State Chem. **179**, 3229 (2006)
12. A.K.H. Nohman, M.I. Zaki, S.A.A. Mansour, R.B. Fahim, C. Kappenstein, Thermochim. Acta **210**, 103 (1992)
13. B. Donkova, D. Mehandjiev, Thermochim. Acta **421**, 141 (1993)

14. F. Gao, R.A. Lewis, X.L. Wang, S.X. Dou, J. Alloys Compd. **347**, 314 (2002)
15. M. Itoh, T. Shimura, J.D. Yu, T. Hayashi, Y. Inaguma, Phys. Rev. B **52**, 12522 (1995)
16. H.Y. Hwang, S.W. Cheong, P.G. Radaelli, M. Marezio, B. Batlogg, Phys. Rev. Lett. **75**, 914 (1995)
17. P. Kameli, H. Salamati, A. Aezami, J. Alloys Compd. **450**, 10 (2008)
18. L.E. Hueso, P. Sande, D.R. Miguens, J. Rivas, F. Rivadulla, M.A. Lopez-Quintela, J. Appl. Phys. **91**, 9943 (2002)
19. R.D. Sanchez, J. Rivas, P. Vaqueiro, M.A. Lopez-Quintela, D. Caeiro, J. Magn. Magn. Mater. **247**, 96 (2002)
20. R.D. Sanchez, J. Rivas, D. Caeiro, M. Ostlund, M. Servin, C. Vazquez, M.A. Lopez-Quintela, M.T. Causa, S.B. Oseroff, Mater. Sci. Forum. **235–238**, 831 (1997)